

*****Copyright Notice*****

No further reproduction or distribution of this copy is permitted by electronic transmission or any other means.

The user should review the copyright notice on the following scanned image(s) contained in the original work from which this electronic copy was made.

Section 108: United States Copyright Law

The copyright law of the United States [Title 17, United States Code] governs the making of photocopies or other reproductions of copyrighted materials.

Under certain conditions specified in the law, libraries and archives are authorized to furnish a photocopy or other reproduction. One of these specified conditions is that the reproduction is not to be used for any purpose other than private study, scholarship, or research. If a user makes a request for, or later uses, a photocopy or reproduction for purposes in excess of "fair use," that use may be liable for copyright infringement.

This institution reserves the right to refuse to accept a copying order if, in its judgement, fulfillment of the order would involve violation of copyright law. No further reproduction and distribution of this copy is permitted by transmission or any other means.

Using Layered Geometry Green's Functions in the Multiple Multipole Program

Aytaç Alparslan* and Christian Hafner

Laboratory for Electromagnetic Fields and Microwave Electronics, ETH Zurich, 8092, Zurich, Switzerland

A new expansion set, layered geometry Green's functions, is introduced in the Multiple Multipole Program (MMP) contained in OpenMaX. It is shown that, with the new expansions, since the necessity of matching the boundary conditions in the layered geometry is eliminated, the complexity of the problems including layered geometries is decreased. Some hints for the derivation of the layered geometry Green's functions and for using them in the OpenMaX package are provided. The robustness and the efficiency of the new expansions are illustrated by various numerical examples, including layered geometries that support guided waves and surface plasmon polaritons (SPP).

Keywords: Multiple Multipole Program (MMP), Layered Geometries, Green's Functions.

1. INTRODUCTION

Lately, the improvements in nanotechnology made it possible to fabricate resonating structures with sizes comparable with the wavelength of the visible spectrum. In the literature, a vast number of applications are analyzed in the optics range by tailoring the shape and material properties of the resonant structures including photonic crystals,^{1–3} chemical and bio-sensors,^{4,5} optical antennas and waveguides^{6–8} and so on. Usually, these devices are fabricated on a substrate or, in the more general case, in a multilayered structure. In the literature, the substrate is often ignored for reasons of simplicity. This may lead to substantial inaccuracies and it may even suppress strong effects such as field singularities in the triple points on the substrate. Furthermore, the layered geometry may support guided waves that are highly important. In order to understand the related physical phenomena and to improve the efficiency of the devices, it is crucial to analyze nano structures within layered geometries numerically. In this paper, the triple point problem and the guided waves are addressed in detail together with numerical examples.

One of the most reliable and efficient simulation tools for the analysis of photonic structures is OpenMaX, which is an open-source program containing the semi-analytic MMP solver.^{9,10} MMP uses arbitrary superpositions of analytic solutions of the Maxwell equations or so called expansions (e.g., plane waves, cylindrical waves, spherical

waves, etc.). In a specific domain i one expands the electromagnetic field (F_i) as follows:

$$F_i = \sum_{n=1}^{N_i} A_n^i E_n^i + \text{error} \quad (1)$$

where E_n^i are the expansions responsible for domain i and A_n^i are the corresponding amplitudes to be determined in such a way that the error is minimized. As a result, the Maxwell equations are fulfilled inside domain i analytically and the accuracy of the results maybe monitored easily on the boundaries by comparing the analytical boundary conditions and the fields generated by the responsible expansions.^{11,12} For simple problems, the routines available in OpenMaX may be used to distribute the expansions for the given boundaries. But in the case of complex problems the types and the locations of the expansions may not be trivial and experience of the user may be needed. One class of such complex problems is the analysis of structures within layered geometries. Since the size of the layered geometries is very large compared with the wavelength, they are taken as infinite structures in the lateral direction. In the MMP analysis of such structures, a geometry truncation is needed in the lateral direction, when using standard single domain expansions (i.e., expansions responsible for the field approximation in only one domain). Then a careful analysis of the errors on the boundaries together with carefully chosen specifications of the expansions is needed in order to obtain reasonably accurate results. In addition, depending on the

*Author to whom correspondence should be addressed.

combinations of the thicknesses and physical properties of the layers, the layered geometry may support guided waves, which makes the MMP modeling even harder, if not impossible.¹³ In order to eliminate the major difficulties listed above when solving problems involving layered geometries, a new expansion type called layered geometry Green's function is introduced. By using these new expansions, the boundary conditions along the boundaries of the layered geometry are fulfilled analytically without any additional expansions, and as the result:

- (1) no explicit discretization of the boundaries of the layered geometry is needed,
- (2) no truncation of layers is needed,
- (3) structures supporting guided wave modes can be simulated
- (4) the problem is solved by a smaller MMP matrix, and
- (5) the fields inside all the domains of the layered geometry (outside of the scatterers) are obtained by using the same set of layered geometry expansions.

Since the intention of this work is to use layered geometry Green's functions as a new expansion set in MMP, a brief discussion of layered geometry Green's functions together with some hints for using them in OpenMaX are provided in Section 2. In Section 3, various examples are analyzed to show that the layered geometry Green's functions can be used in a robust way in the solution of electromagnetic problems.

Delivered by Publishing Technology to University of Houston
IP: 129.7.158.43 On: Tue, 01 Mar 2016 20:22:28
Copyright: American Society of Mechanical Engineers

2. LAYERED GEOMETRY GREEN'S FUNCTIONS

The Green's function in electromagnetics is the response of the system to a fundamental point source. In free space the Green's functions are planar, cylindrical and spherical waves in 1D, 2D and 3D respectively. Since these kind of waves can be analytically formulated, it is easy and fast to use them in numerical methods, such as in MMP. But in the case of layered geometries, since there is no analytic expression for the Green's function in 2D and 3D, one needs to write the content of the Green's functions as a superposition of orthogonal set of functions (e.g., sines, cosines, complex exponentials, etc...), of which the distinct response of the layered geometry can be obtained analytically. Then the Green's function is obtained by summing up all the contributions of the functions in the orthogonal set chosen. Since the spectrum of the point source is infinite and continuous, the summation leads to an integration with infinite bounds, which is called the Sommerfeld Integral.^{14, 15} As an example, for the general layered geometry shown in Figure 1 the following integration must be calculated (Hankel or inverse Fourier transform) to obtain the Green's function (in this paper $e^{-i\omega t}$ time convention is used).

$$G^{2D}(x, y) = \frac{1}{2\pi} \int_{-\infty}^{\infty} dk_x e^{ik_x x} \tilde{G}^{2D}(k_x)$$

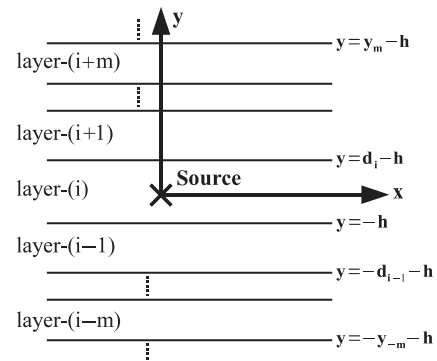


Fig. 1. General multilayered geometry. The source is a line source (monopole) in 2D and a point source (dipole) in 3D.

$$G^{3D}(\rho, y) = \frac{1}{4\pi} \int_{-\infty}^{\infty} dk_{\rho} k_{\rho} H_0^{(1)}(k_{\rho}\rho) \tilde{G}^{3D}(k_{\rho}) \quad (2)$$

where G^{nD} and \tilde{G}^{nD} are the spatial domain (space) and spectral domain (spectrum) Green's functions in n dimensional space respectively, $H_0^{(1)}$ is the Hankel function of the first kind and ρ is the lateral distance from the source (i.e., $\rho = \sqrt{x^2 + z^2}$ for the coordinate system in Fig. 1).

In (2), the integration has infinite bounds (starting from $-\infty$, following the real axis up to $+\infty$) and has no analytical solution. Therefore a numerical integration must be adopted in order to obtain the spatial domain Green's functions. The two major problems with this numerical integration scheme can be listed as:

- (1) the infinite bounds and
- (2) possible singularities due to guided wave modes on or near (when losses are present) the real axis.

In order to tackle these problems, the integration path is modified as shown in Figure 2, which is called the Sommerfeld Integration Path (SIP). This modification is allowed mathematically, since the causality principle is not violated (Ref. [15] i.e., the path should not cross the branch points and cuts and guided wave singularities). According to Figure 2, the integration on the path between $-k_m \rightarrow k_m$ is obtained directly by using a numerical integrator, since there are no singularities on the path (a period of a weighted sine function is used as the path between $-k_m$ and k_m here). The remaining parts (i.e., the integrals

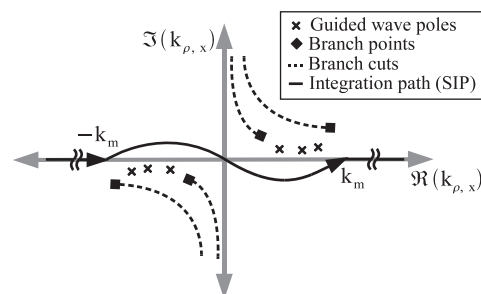


Fig. 2. Sommerfeld integration path and the locations of possible singularities.

with the bounds $-\infty \rightarrow -k_m$ and $k_m \rightarrow \infty$) are integrated by using series acceleration techniques as described in Ref. [16].

In order to obtain the spatial domain Green's functions in a robust way for any kind of layered geometry, it is necessary to analyze the k_m value in the numerical integration scheme given above. In layered geometries that include only dielectrics, it is guaranteed that all the singularity locations have a real part that is less than the wave number of the densest medium in the layered geometry (physically, the real part of the wave number of a guided wave mode can not exceed the wave number of the material with the highest refractive index in the layered geometry). Therefore, for layered geometries that include only dielectric materials, setting the k_m value equal to the highest wave number in the layered geometry guarantees that there are no singularities in any part of the path shown in Figure 2. But in the case of layered geometries including plasmonic structures, the locations of the SPP singularities can be at any location depending on the thicknesses of the metallic layers, therefore a more careful analysis of the spectral domain Green's function may be needed.¹⁷ Usually, taking k_m equal to 3 times the highest wave number of the layered geometry is enough for most of the applications. But, one should be careful when simulating structures including layered geometries with very thin (e.g., $< \lambda_0/20$) metallic layers. For such structures, the location of the highest SPP wave number should be evaluated and a suitable k_m value should be determined, since very high k_m values would increase the computation time of the integration. In OpenMaX, a variable called "Sommerfeld k " is introduced in order to control the bounds of the integration path. In the solution of geometries that include layered geometries made of dielectrics only, it is safe to set "Sommerfeld k " equal to 1. For layered structures including metals, it is enough to set "Sommerfeld k " equal to 3 for most of the applications, but the user should be still careful due to the reasons outlined above.

When taking the inverse Fourier transform in 2D as in (2), the field generated by the line source is obtained as a sum of plane waves in both the lateral ($e^{ik_x x}$ terms) and vertical (included in $\tilde{G}^{2D}(k_x)$)¹⁸ directions. Also in 3D, when taking the Hankel transform as in (2), the field generated by a point source is obtained as a sum of cylindrical waves in the lateral direction ($H_0^{(1)}(k_\rho \rho)$ terms) and plane waves (included in $\tilde{G}^{3D}(k_x)$)¹⁸ in the vertical direction. Choosing plane waves in the vertical direction is because of the fact that the response of the layered geometry to the plane wave with a given wave number can be obtained analytically, which makes it possible to obtain the spectral domain Green's functions.^{15, 18, 19} Unfortunately the integrands in (2) are oscillatory and slowly decaying in general, which makes the integration a time consuming process. The singularities close to the integration path make it even harder to obtain the results.^{16, 20} In

order to obtain the Green's functions in an efficient way, several techniques were introduced,^{21, 22} which are applicable to geometries with a single branch point in the spectral domain Green's function (i.e., to be able to use these methods, the layers on the top and bottom must be the same resulting in a single branch point in the spectral domain). However in the optics regime, since there are 2 branch points in most of the applications (as in the case of substrates), these methods cannot be used. In order to increase the speed of the integrations, an "adaptive simultaneous integration routine," which was readily available in OpenMaX, is used to integrate similar components.¹⁰ Since the common quantities like the reflection/transmission coefficients and amplitude transfer functions are evaluated only once for similar integrands, the integration time is significantly ($\sim \times 3$ in 2D and $\sim \times 8$ in 3D) reduced. This made it possible to use the layered geometry Green's functions as a new expansion set in OpenMaX without any restrictions concerning material properties of the top and bottom layers.

3. NUMERICAL EXAMPLES

3.1. Scatterer Inside a Multilayered Geometry

As first example, a triangular scatterer made of silver ($\epsilon_{r, Ag} = -15.91 + 0.43i$) is placed inside a 2D layered geometry setting as shown in Figure 3 together with the locations and types of the expansions used. The vertices of the scatterer are placed at (0 nm, 80 nm), (80 nm, -80 nm) and (-80 nm, -80 nm) and the radius of curvature is taken to be 30 nm for all the vertices. It must be noted that the distributions of the expansions are obtained by the automatic multipole setting routine available in OpenMaX. In order to obtain an average relative error below 0.5%, 25 multilayer expansions and 25 multipoles with the maximum order of 2 are used. The multilayer expansions model the field in all the layers outside the scatterer, whereas the multipoles model the field inside the scatterer. The free-space wavelength of the field generated by the line source at (0 nm, 200 nm) that excites the structure is 600 nm.

(1) *Scatterer inside a dielectric substrate:* As the first example, the first 4 layers in Figure 3 are set to be a dielectric material with $\epsilon_r = 9.0$ and layer 5 is taken to be free-space. The resulting field distributions when the line source is taken as an electric (E_z polarization) and magnetic (H_z polarization) monopole can be seen in Figures 4(a) and (b) respectively.

As illustrated in the results, a surface plasmon resonance is generated around the metallic scatterer in the H_z polarization case, whereas no surface plasmon is generated in the E_z polarization case, since only the permittivity value of the metal has a negative real part.

(2) *Scatterer inside a dielectric slab:* As the second example, a layered structure that supports guided waves is

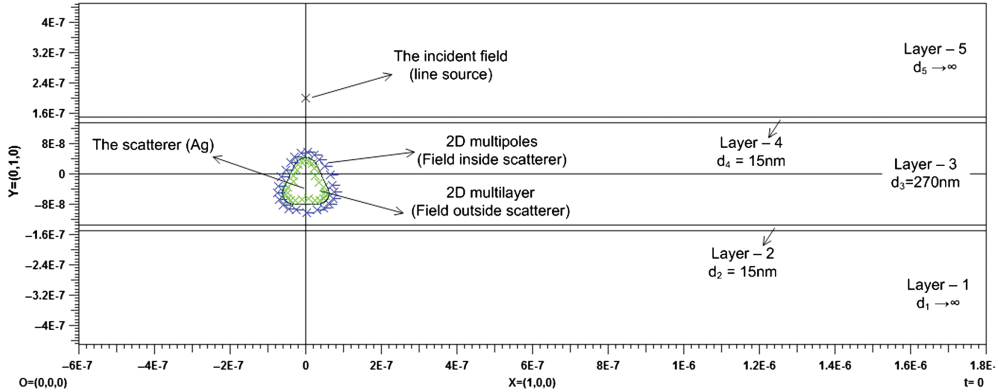


Fig. 3. The general setting for example 1: A 5-layered geometry with the locations of the expansions and corresponding thickness values for the layers.

selected as follows: Layers 1, 2, 4 and 5 are free space and layer 3 is dielectric with $\epsilon_r = 9.0$ according to the setting shown in Figure 3. The resulting field distributions when the line source is taken as an electric (E_z polarization) and magnetic (H_z polarization) monopole can be seen in Figures 5(a) and (b) respectively.

Here, the results are similar to the previous one, in terms of surface plasmon generation, i.e., in H_z polarization,

a surface plasmon resonance is observed. The difference between the first simulation and the current one is that the dielectric slab in the current simulation allows guided wave modes to propagate inside the slab, resulting in a higher concentration of fields, as seen in Figure 5. It is also worth noting that there are 3 guided wave modes both in E_z and H_z polarizations with the following wave numbers in the direction of propagation

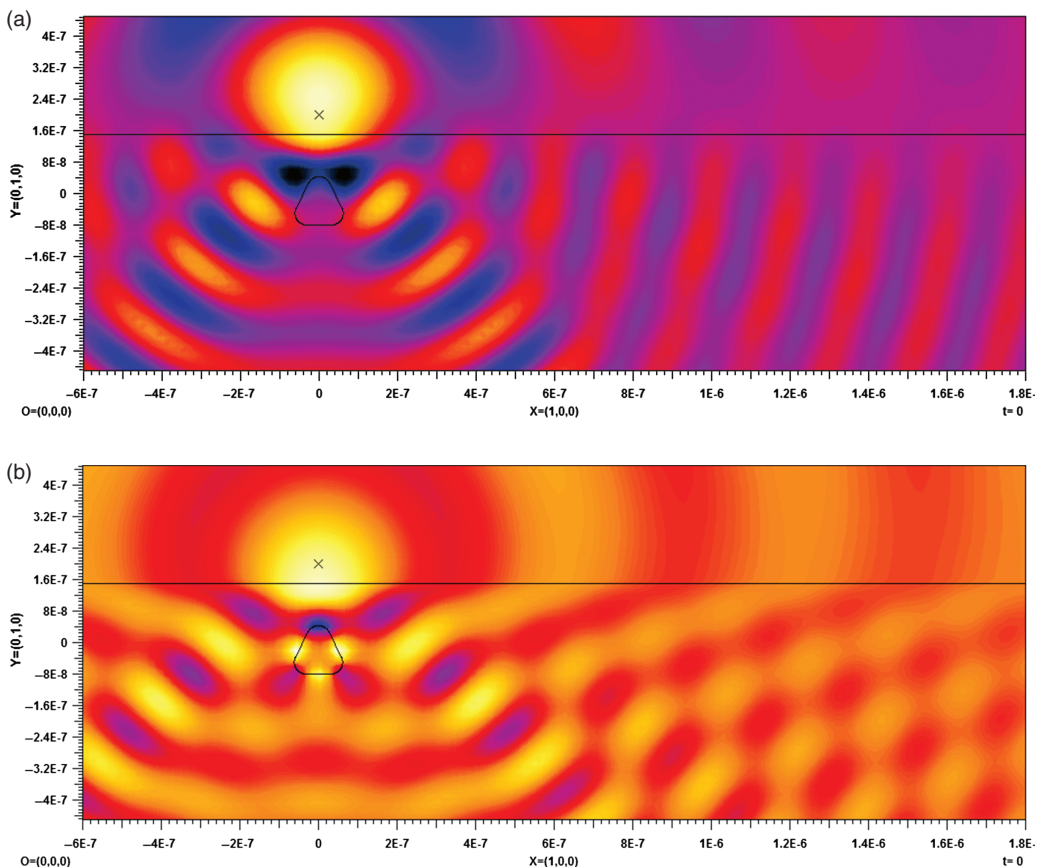


Fig. 4. Results of the simulation with a triangular Ag scatterer inside a dielectric substrate with $\epsilon_r = 9.0$. (a) E -field, z -component (Arbitrary units). Incident field: An electric monopole with $\lambda_0 = 600$ nm at the location of the black cross. (b) H -field, z -component (Arbitrary units). Incident field: A magnetic monopole with $\lambda_0 = 600$ nm at the location of the black cross.

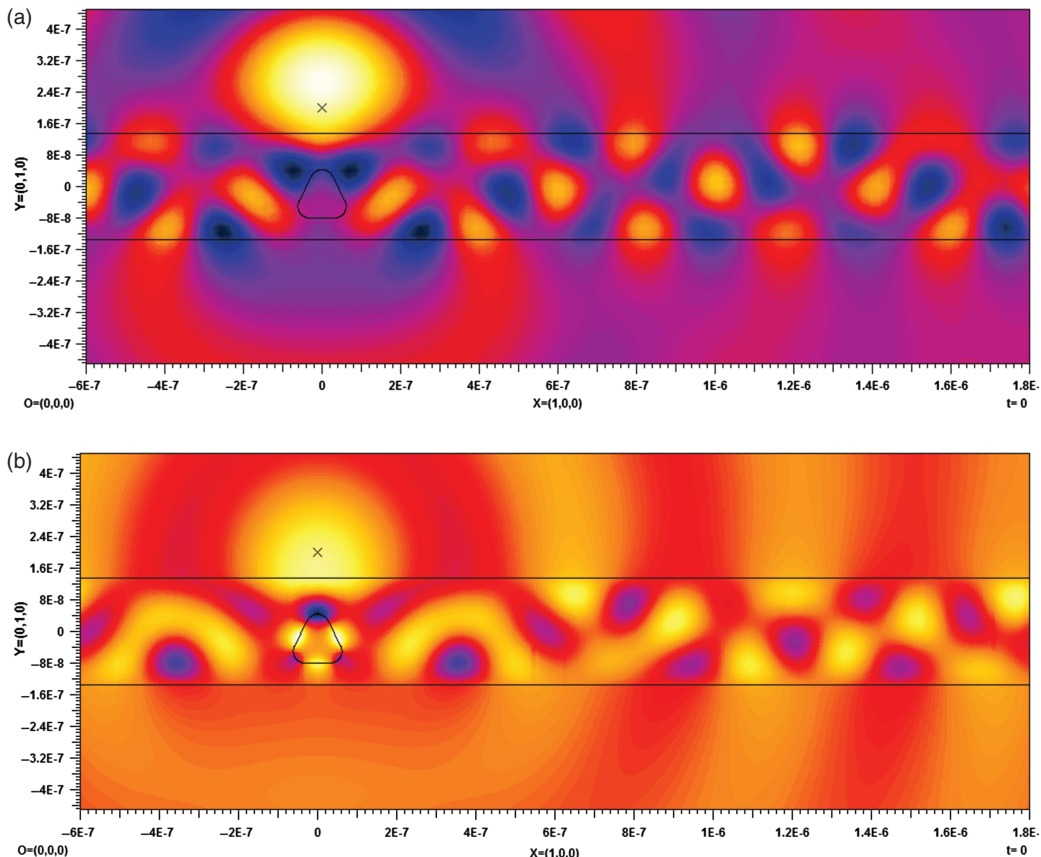


Fig. 5. Results of the simulation with a triangular Ag scatterer inside a slab with $\epsilon_r = 9.0$ and thickness of 270 nm. (a) E -field, z -component (Arbitrary units). Incident field: An electric monopole with $\lambda_0 = 600$ nm at the location of the black cross. (b) H -field, z -component (Arbitrary units). Incident field: A magnetic monopole with $\lambda_0 = 600$ nm at the location of the black cross.

(x -direction): $k_{1,E_z} = 1.5919k_0$, $k_{2,E_z} = 2.4365k_0$, $k_{3,E_z} = 2.8662k_0$, $k_{1,H_z} = 1.05616k_0$, $k_{2,H_z} = 2.1101k_0$ and $k_{3,H_z} = 2.7994k_0$ with k_0 being the free-space wave number of the incident field. As discussed in Section 2, for this problem, the variable “Sommerfeld k ” should be set to 1 in order to guarantee that the SIP does not cross any of the singularities listed above. The exact locations of the singularities are listed here to demonstrate that the choice of the SIP shown in Figure 2 together with the variable “Sommerfeld k ” makes the integration robust and eliminates the necessity of knowing the exact locations of the singularities.

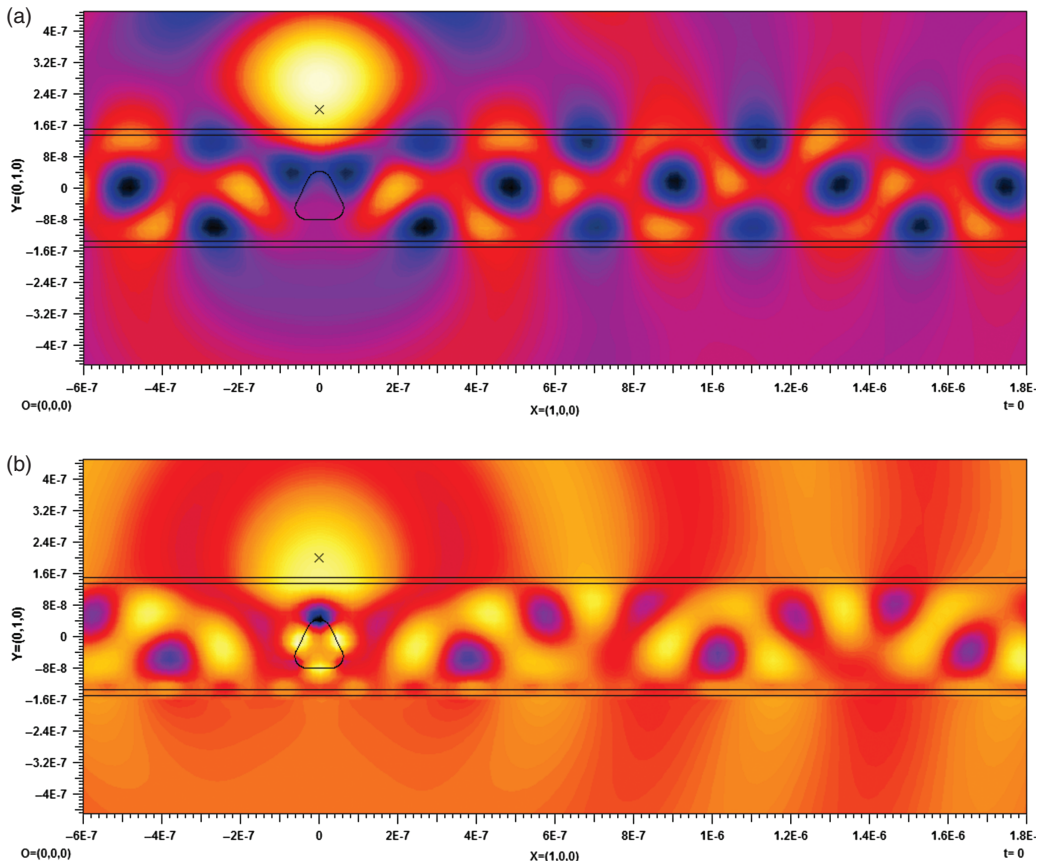
(3) *Scatterer inside a general multilayered geometry:* For the last example using the setting seen in Figure 3, the following parameters are used: layer 1 and layer 5 are free-space, layer 2 is silver, layer 3 and layer 4 are dielectric with $\epsilon_{r3} = 9.0$ and $\epsilon_{r4} = 2.0$, respectively. The resulting field distributions when the line source is taken as an electric (E_z polarization) and magnetic (H_z polarization) monopole can be seen in Figures 6(a) and (b) respectively.

As shown in Figure 6, the results are very similar to the previous one. Again, 3 guided wave modes are found both in E_z and H_z polarizations with the following wave numbers: $k_{1,E_z} = (1.4256 + 0.0032i)k_0$, $k_{2,E_z} = (2.3898 + 0.0008i)k_0$, $k_{3,E_z} = (2.8567 + 0.0002i)k_0$,

$k_{1,H_z} = (1.0483 + 0.0010i)k_0$, $k_{2,H_z} = (1.9330 + 0.0048i)k_0$ and $k_{3,H_z} = (2.7634 + 0.0010i)k_0$ with k_0 being the free-space wave number of the incident field. Due to the shift in the guided wave modes, the field distribution is slightly changed inside the dielectric slab. In addition to this difference, one can see the coupling of SPPs between the scatterer and the metallic layer in H_z polarization. Since the metallic layer is very thin compared to the wavelength of the incident field, the wave number of the SPP generated on the surface is shifted (in a semi-infinite dielectric ($\epsilon_r = 9.0$)-Ag ($\epsilon_{r,Ag} = -15.91 + 0.43i$) interface, the wave number of the SPP would be $k_{SPP} = (4.5479 + 0.0799i)k_0$), resulting in a maximum SPP wave number of $k_{SPP,max} = (5.9978 + 0.1505i)k_0$ as described in Ref. [17]. Therefore, setting “Sommerfeld k ” value equal to 3 is sufficient to obtain the spatial domain Green’s functions even for this rather extreme example.

3.2. Scatterer on Top of a Multilayered Geometry (Triple Point Problem)

In the second example, a rectangular scatterer made of silver ($\epsilon_{r,Ag} = -15.91 + 0.43i$) is placed on top of a layered geometry as seen in Figure 7, together with the locations



IP: 129.7.158.43 On: Tue, 01 Mar 2016 20:01:28

Fig. 6. Results of the simulation with a triangular Ag scatterer inside a general multilayered setting with the following specifications: Layer-1 and Layer-5 are free-space, Layer-2 is silver, Layer-3 and Layer-4 are dielectric with $\epsilon_{r3} = 9.0$ and $\epsilon_{r4} = 2.0$. (a) E -field, z -component (Arbitrary units). Incident field: An electric monopole with $\lambda_0 = 600$ nm at the location of the black cross. (b) H -field, z -component (Arbitrary units). Incident field: A magnetic monopole with $\lambda_0 = 600$ nm at the location of the black cross.

of the expansions used. The vertices of the scatterer are placed at $(-130$ nm, 200 nm), $(-130$ nm, 330 nm), $(130$ nm, 330 nm) and $(130$ nm, 200 nm) and the radius of curvature is taken to be 30 nm for all the vertices. For the examples given by using this setting, 45 multilayer expansions and 45 multipoles with the maximum order of 2 are used, which results in an average relative error less than 0.5% in all the cases. The free-space

wavelength of the field generated by the line source at $(-900$ nm, 900 nm) that excites the structure is 600 nm. This example is interesting in the sense that there are some sections in the boundary of the scatterer, called triple points, where three different domains come together. In triple points the field may exhibit field singularities that may not be lifted by smoothing procedures. This leads to demanding numerical problems. In the following examples

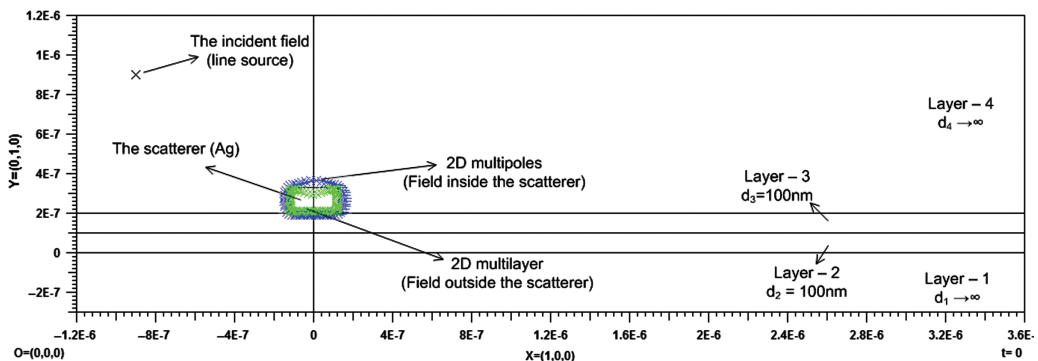


Fig. 7. The general setting for example 2: A 4-layered geometry with the locations of the expansions and corresponding thickness values for the layers.

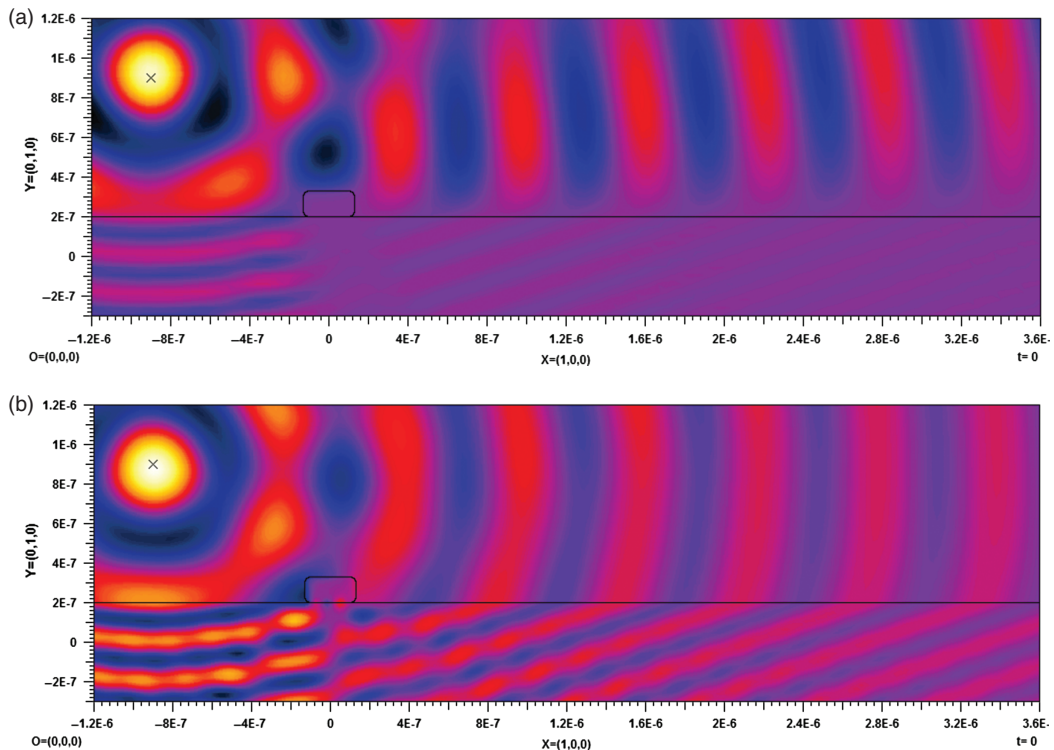


Fig. 8. Results of the simulation with a rectangular Ag scatterer on top of a dielectric substrate with $\epsilon_r = 9.0$. (a) E-field, z-component (Arbitrary units). Incident field: An electric monopole with $\lambda_0 = 600$ nm at the location of the black cross. (b) H-field, z-component (Arbitrary units). Incident field: A magnetic monopole with $\lambda_0 = 600$ nm at the location of the black cross.

Downloaded by: University of Houston
IP: 129.7.158.43 On: Tue, 01 Mar 2016 20:01:28
Copyright: American Scientific Publishers

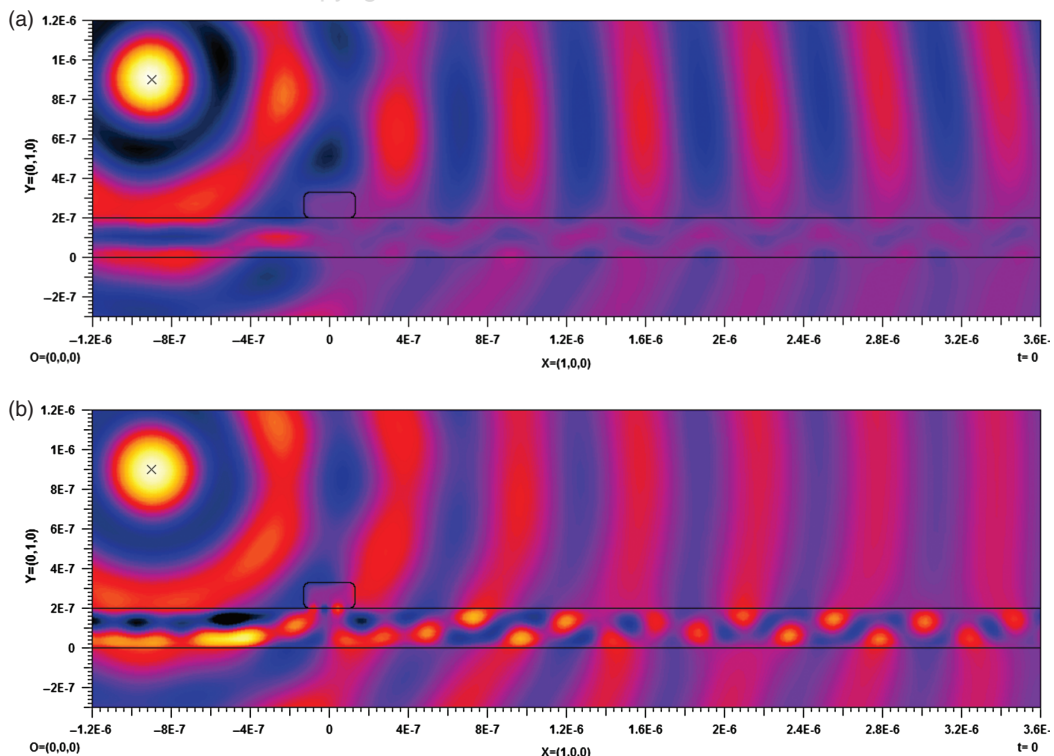


Fig. 9. Results of the simulation with a rectangular Ag scatterer on top of a dielectric slab with $\epsilon_r = 9.0$. (a) E-field, z-component (Arbitrary units). Incident field: An electric monopole with $\lambda_0 = 600$ nm at the location of the black cross. (b) H-field, z-component (Arbitrary units). Incident field: A magnetic monopole with $\lambda_0 = 600$ nm at the location of the black cross.

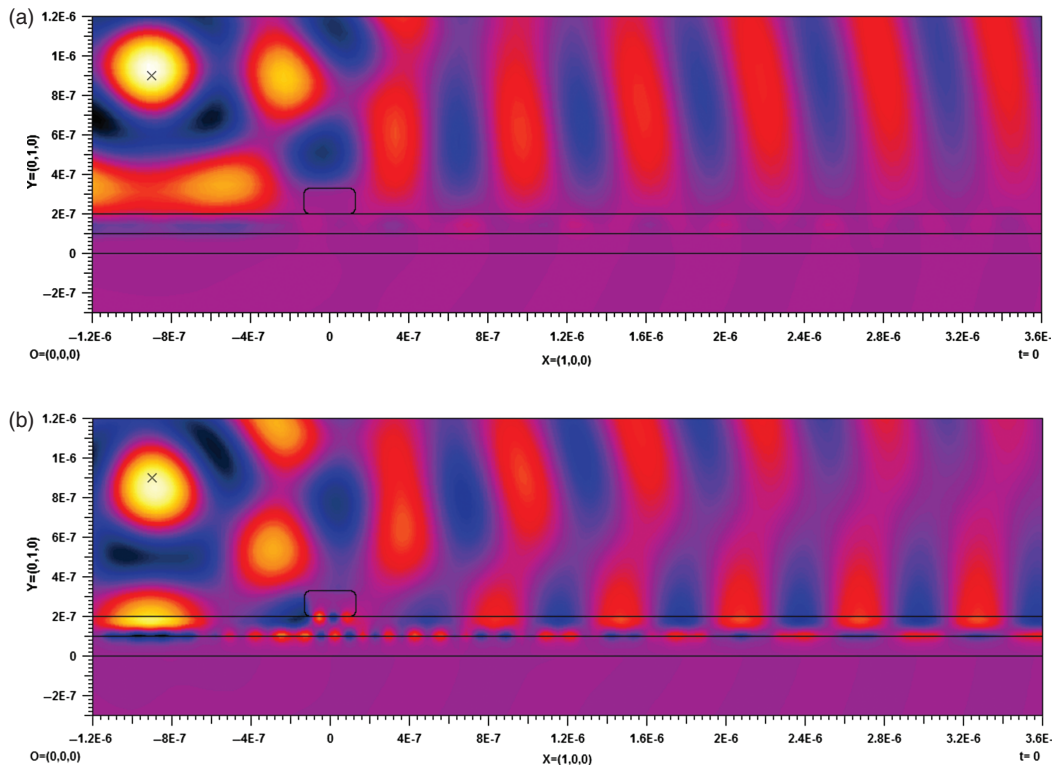


Fig. 10. Results of the simulation with a rectangular Ag scatterer on top of a Ag backed dielectric slab with $\epsilon_r = 9.0$. (a) E -field, z -component (Arbitrary units). Incident field: An electric monopole with $\lambda_0 = 600$ nm at the location of the black cross. (b) H -field, z -component (Arbitrary units). Incident field: A magnetic monopole with $\lambda_0 = 600$ nm at the location of the black cross.

it will be illustrated that the boundary conditions are correctly fulfilled by OpenMaX for this kind of structures as well.

(1) *Scatterer on top of a dielectric substrate:* For the first example using the setting in Figure 7 the following specifications are used: the first 3 layers are dielectric materials with $\epsilon_r = 9.0$ and layer 4 is free-space. The resulting field distributions when the line source is taken as an electric (E_z polarization) and magnetic (H_z polarization) monopole can be seen in Figures 8(a) and (b) respectively.

As one can see, the H_z polarization case differs from the E_z polarization case by the generation of SPP on the surface of the scatterer. It is also worth noting that two different SPPs are seen on the scatterer: one on the boundary neighboring to free-space and the other on the boundary to the dielectric substrate. These two different waves are correctly matched on the same scatterer, demonstrating that structures including layered geometries with triple points can be simulated by OpenMaX.

(2) *Scatterer on top of a dielectric slab:* As the second example, a layered structure that supports guided waves is selected as follows: layers 1 and 4 are free-space and layers 2 and 3 are dielectric with $\epsilon_r = 9.0$ according to the setting shown in Figure 7. The resulting field distributions when the line source is taken as an electric (E_z polarization) and magnetic (H_z polarization) monopole can be seen in Figures 9(a) and (b) respectively.

As expected, a field localization is observed in the dielectric slab, since the layered geometry can support guided waves. For this example 2 guided waves are supported both in E_z and H_z polarizations, with the following wave numbers: $k_{1,E_z} = 2.0750k_0$, $k_{2,E_z} = 2.7857k_0$, $k_{1,H_z} = 1.3325k_0$ and $k_{2,H_z} = 2.6332k_0$.

(3) *Scatterer on top of a general multilayered geometry:* For the last example, the scatterer is placed on top of a metal backed dielectric slab with the following specifications: layer 1 and 4 are free-space, layer 2 is silver with $\epsilon_{r,Ag} = -15.91 + 0.43i$ and layer 3 is dielectric with $\epsilon_r = 9.0$. The resulting field distributions when the line source is taken as an electric (E_z polarization) and magnetic (H_z polarization) monopole can be seen in Figures 10(a) and (b) respectively.

In this example, since the slab is backed by a metal, a coupling of SPP is observed between the scatterer and metal layer. Also a guided wave mode is observed both in E_z and H_z polarizations, with the following wave numbers: $k_{1,E_z} = (2.3099 + 0.0017i)k_0$ and $k_{1,H_z} = (1.01481 + 0.0005i)k_0$, with k_0 being the free-space wave number of the incident field. The wave number of the SPP generated on the Ag layer is $k_{SPP} = (4.5479 + 0.0799i)k_0$, which is the same as the wave number of the SPP that would be generated in a semi-infinite dielectric ($\epsilon_r = 9.0$)-Ag ($\epsilon_{r,Ag} = -15.91 + 0.43i$) interface, since the metallic layer is thick enough.

4. CONCLUSIONS

In this paper, the implementation of layered geometry Green's functions as a new expansion set for OpenMaX is described and applied. Starting with a brief discussion of layered geometry Green's functions both in the spectral and spatial domains, several difficulties in the Sommerfeld integration, i.e., transformation from spectral to spatial domain, and hints to tackle them are given. Then, the implementation of the new expansion set is explained. Finally, several numerical examples including dielectric and metallic layers with various combinations of scatterers are introduced and analyzed in 2D, since the insertion of 3D layered Green's functions was still under construction at the time of the publication. Usually the application of MMP in 3D is more demanding computationally but, since the boundary matching procedure in 2D and 3D are quite similar, the numerical examples demonstrate the robustness and efficiency of the new expansions. As the result, OpenMaX became a more user-friendly and efficient simulation tool when dealing with layered geometries, since the necessity of matching the boundary conditions by standard expansions in the layered geometries is eliminated.

References

1. J. D. Joannopoulos, P. R. Villeneuve, and S. Fan, *Solid State Commun.* 102, 165 (1997).
2. S. G. Johnson, S. Fan, P. R. Villeneuve, J. D. Joannopoulos, and L. A. Kolodziejski, *Phys. Rev. B* 60, 5751 (1999).
3. J. Smajic, C. Hafner, and D. Erni, *Opt. Express* 11, 1378 (2003).
4. T. Sannomiya, C. Hafner, and J. Vörös, *Journal of Biomedical Optics* 14, 064027 (2009).
5. S. M. Borisov and O. S. Wolfbeis, *Chem. Rev.* 106, 423 (2008).
6. P. Mühlischlegel, H. Eisler, O. J. F. Martin, B. Hecht, and D. W. Pohl, *Science* 308, 1607 (2005).
7. L. Novotny, *Phys. Rev. Lett.* 98, 266802 (2007).
8. P. Bharadwaj, B. Deutsch, and L. Novotny, *Adv. Opt. Photon.* 1, 438 (2009).
9. C. Hafner and N. Kuster, *Radio Science* 26, 291 (1991).
10. OpenMaX. Available: <http://openmax.ethz.ch/>.
11. C. Hafner, Generalized Multipole Technique for Computational Electromagnetics, ser. Artech House Antenna Library, Artech House, Boston, MA (1990).
12. C. Hafner, *Physica Status Solidi (b)* 244, 3435 (2007).
13. T. Sannomiya and C. Hafner, *Journal of Computational and Theoretical Nanoscience* 7, 1587 (2010).
14. N. Felsen and L. B. Marcuvitz, Radiation and Scattering of Waves, John Wiley and Sons, (1994).
15. W. C. Chew, Waves and Fields in Inhomogeneous Media, Van Nostrand Reinhold, New York (1990).
16. K. A. Michalski, *IEEE Trans. Antennas Propag.* 46, 1405 (1998).
17. A. Alparslan and M. I. Aksun, *Proceedings of IEEE Photonics-Global@Singapore* 1 (2008).
18. G. Dural and M. I. Aksun, *IEEE Trans. Microw. Theory Tech.* 43, 1545 (1995).
19. N. Kinayman and M. I. Aksun, Modern Microwave Circuits, Artech House, Norwood, MA (2005).
20. M. I. Aksun and G. Dural, *IEEE Trans. Antennas and Propag.* 53, 3644 (2005).
21. A. Alparslan, M. Aksun, and K. Michalski, *IEEE Trans. Microw. Theory Tech.* 58, 602 (2010).
22. A. G. Polimeridis, T. V. Yioultsis, and T. D. Tsiboukis, *IEEE Trans. Antennas Propag.* 55, 1963 (2007).

Received: 20 September 2010. Accepted: 15 October 2010.